

# LMC X-2: The First Extragalactic $Z$ -Source?

Alan P. Smale<sup>1</sup>

*Laboratory for High Energy Astrophysics, Code 662, NASA/Goddard Space Flight Center, Greenbelt, MD 20771*

Erik Kuulkers

*Space Research Organization Netherlands, Sorbonnelaan 2, 3584 CA Utrecht<sup>2</sup>*

## ABSTRACT

We present RXTE observations of LMC X-2 obtained during a five-day interval in 1997 December, during which the source was radiating at a mean intensity near the Eddington limit, and strongly variable on timescales of seconds to hours. The shapes of the X-ray color-color and hardness-intensity diagrams during the observations, the presence of VLFN and HFN in the power spectra, and the high intrinsic X-ray luminosity of LMC X-2 (which historically spans  $0.4-2.0L_{Edd}$  for reasonable estimates of the neutron star mass) are more characteristic of a  $Z$ -source in its flaring branch than of an atoll-source. On this basis, we provisionally reclassify LMC X-2 as a  $Z$ -source, the eighth such source known and the first to be detected beyond our Galaxy.

Using periodogram and Fourier analysis of the X-ray lightcurve we detect an apparently-significant modulation with a period of  $8.160 \pm 0.011$  hrs and a semi-amplitude increasing from 14% in the 1.8–4.0 keV range to 40% at 8.7–19.7 keV. This X-ray modulation appears to confirm a candidate orbital periodicity determined from optical photometry ten years prior to our campaign, but we cannot rule out a chance alignment of intrinsic X-ray flares. Current RXTE ASM light curves and archival EXOSAT observations show no sign of such a pronounced periodicity.

The X-ray spectrum of LMC X-2 can be well fit using variations of simple Comptonization models. Fits to phase( $\simeq$ intensity)-resolved spectra show strong correlations between the power law slope (in one parameterization) or the depth to optical scattering (in another) and phase. We discuss the implications of these results for the inclination, geometry, and emitting regions of the LMC X-2 system.

*Subject headings:* accretion, accretion disks — stars: individual (LMC X-2) — stars: neutron — stars: binaries: close — X-rays: stars

---

<sup>1</sup>Also Universities Space Research Association.

<sup>2</sup>Also Astronomical Institute, Utrecht University, P.O. Box 80000, 3507 TA Utrecht, The Netherlands.

## 1. Introduction

Considering its extreme brightness, it is perhaps surprising how little is known about LMC X-2 (0521–720). One of the most luminous persistent sources in the Large Magellanic Cloud, it is the only one of these original five bright X-ray sources to be identified as a low mass X-ray binary (LMXB). With an observed X-ray luminosity in the range  $0.6\text{--}3\times 10^{38}$  erg s<sup>-1</sup> (van Paradijs 1995), LMC X-2 has a persistent emission which can exceed the Eddington luminosity for a neutron star with a canonical mass of  $1.4\text{--}2.0M_{\odot}$ , making it one of the most powerful persistently-emitting low mass X-ray binaries. Because of its accurately-known distance and low line-of-sight absorption, studies of LMC X-2 can provide not only a clear view of the physics and dynamics of such a system, but also an important comparison with Galactic LMXBs.

The spectrum of the  $V=18.8$  optical counterpart (Johnston et al. 1979) shows the expected strong He II emission overlying a blue continuum, but the N III–C III–O II blend emission typically seen at  $\lambda\lambda 4640\text{--}4650\text{\AA}$  is weak or non-existent (Bonnet-Bidaud et al. 1989; Crampton et al. 1990). The Bowen blend is also absent in the optical spectra from the supersoft LMC sources, indicating that the lack of this emission is linked to the relatively low metallicity of the LMC. This underabundance may also contribute to the high luminosities observed in the LMC X-ray sources in general, compared to the Galactic population. Accretion of material onto compact objects may be limited by preheating due to photoelectric absorption of X-rays by the heavier elements in the material, thus sources in a lower-abundance environment might be expected to accrete closer to the Eddington limit.

For LMC X-2 the ratio of X-ray to optical luminosities is  $L_x/L_{opt} \sim 600$ , similar to that seen in Galactic LMXBs. The weakness of the 6.7 keV Fe line (White et al. 1986; Bonnet-Bidaud et al. 1989) supports the lower-abundance argument. Searches for the orbital period of the system have produced contradictory results, with evidence for photometric and/or spectroscopic periods of 6.4 hr (Bonnet-Bidaud et al. 1989), 8.16 hr (Callanan et al. 1990), and 12.5 days (Crampton et al. 1990). Thus, even the nature of the companion and the scale of the binary system are unclear. A 6–8 hr period would imply a late-type dwarf companion, while the longer 12.5-day period would require an evolved companion in a much larger orbit (e.g. Hasinger & van der Klis 1989).

Searches of the literature and the archival holdings at the HEASARC reveal that few dedicated observations of LMC X-2 have been performed. Data from the earlier satellites consist almost entirely of surveys of (or including) the LMC. Flux measurements prior to 1977, and the long-term behavior of the source, are summarized in Griffiths & Seward (1977). The HEAO-1 and Einstein survey data can be found in Johnston, Bradt, & Doxsey (1979) and Long, Helfand, & Grabelsky (1981). A short multiwavelength study of LMC X-2 was conducted by Bonnet-Bidaud et al. (1989), using EXOSAT and the ESO complex at La Silla in 1984. They determined that the X-ray spectra could be described using either a Comptonization model, or the sum of two components, i.e. Bremsstrahlung plus a blackbody. In the first representation, the authors note that their ability to determine the existence or non-existence of a blackbody component was strongly limited by the available statistics. In the second, the blackbody component contributed 20–40% of the total emission, and the blackbody radius was found to be 6–10 km. Variability is typically observed in the light curve on  $\sim 5\text{--}30$  min timescales, and a flare (brightness enhancement) was also seen. However, this flare only represents a 25% increase in the persistent emission at the end of the observation, and is not well modeled by an increase in the blackbody flux in the two-component representation. The EXOSAT observations presented by Bonnet-Bidaud et al. lasted 8.2 hours, too short to effectively search for a period in the 4–12 hr range or beyond. No clear correlation was observed between X-ray and optical emission, and no significant QPO or red noise features were detected in the 2–64 Hz range studied.

Accreting LMXBs can be divided into two classes based on their fast-timing behavior and variations in their spectral color or hardness (Hasinger & van der Klis 1989; for a review, see e.g. van der Klis 1995). The  $Z$ -sources are named for the three-branched shape they trace in a diagram of ‘hard’ color against ‘soft’ color. From top to bottom, the three branches of the  $Z$  are known as the Horizontal, Normal, and Flaring branches (HB, NB, FB), and it is believed that the accretion rate  $\dot{M}$  increases as the source moves from the HB to the FB.

The  $Z$ -sources generally show quasi-periodic oscillations in their powers spectra in the 1–100 Hz range whose characteristics are closely correlated with their position on the  $Z$ . Horizontal Branch QPOs, or

TABLE 1  
OBSERVATION LOG

Observation	Start/Stop Time (UT)
1	1997 Dec 2 18:52 – 1997 Dec 3 02:00
2	1997 Dec 3 19:07 – 1997 Dec 4 02:00
3	1997 Dec 4 18:53 – 1997 Dec 5 01:59
4	1997 Dec 5 19:20 – 1997 Dec 6 02:00
5	1997 Dec 6 18:51 – 1997 Dec 7 01:40

HBOs, are probably explained by a magnetospheric beat frequency model, while Normal/Flaring branch QPOs (N/FBOs) are related to oscillations in the accretion flow near/beyond the Eddington limit. In addition, the power spectra show power-law shaped noise at frequencies  $\gtrsim 1$  Hz (known as very low frequency noise, or VLFN); band-limited ( $\sim 1$ –10 Hz) noise with cut-off frequencies of  $\sim 10$  Hz (called low-frequency noise, LFN) in the Horizontal and upper part of the Normal branch; and high-frequency noise (HFN) with cut-off frequencies in excess of 50–100 Hz, which sometimes leads to a broad, peaked appearance. The currently-known  $Z$ -sources are Sco X-1, GX 17+2, GX 349+2 (=Sco X-2), Cyg X-2, GX 340+0, and GX 5-1 (Hasinger & van der Klis 1989). When bright, Cir X-1 also shows  $Z$ -source characteristics (Shirey et al. 1998; Shirey, Bradt & Levine 1999).

The second class, the so-called ‘atoll’ sources, describe a much simpler curved ‘banana’ shape in their color-color diagram, sometimes supplemented with an ‘island’ of datapoints during low-luminosity intervals. The atoll sources show VLFN with a generally shallower power law index than the  $Z$ -sources, and a broad low-frequency band-limited noise component often (confusingly) also termed HFN.

Both  $Z$ - and atoll sources also display QPO oscillations at frequencies of 200–1200 Hz (“kiloHertz QPOs”, see e.g. van der Klis 1998) and at 1–60 Hz (see e.g. the review of van der Klis 1995 for the  $Z$ -sources, and Wijnands & van der Klis 1999 and references therein for a tabular summary of such oscillations in the atoll sources).

To date the  $Z$ -sources have tended to show longer orbital periods ( $\sim 18$  hrs – 10 days), implying evolved

companions, while atoll sources tend to have orbital periods under 10 hrs. Confirmed membership of one or other class has direct physical consequences for the system; the  $Z$ -source characteristics imply the existence of magnetospheres with magnetic fields of  $B \sim 10^9$ – $10^{10}$ G, while the magnetic fields in the atoll sources would be substantially lower (see Psaltis, Lamb, & Miller 1995). The difference in the nature of the companions possibly implies that  $Z$ - and atoll-sources differ in their evolutionary history (Hasinger & van der Klis 1989).

Assignment of LMC X-2 to one or other of these classes can only be achieved by studying the color-color diagram and the fast time variability of the source. No clear color-color correlation was observed during the EXOSAT observations, but it is apparent from the hardness diagrams presented by Bonnet-Bidaud et al. (1989) that the low-level variability analysis was affected by the counting statistics. Despite its absolute brightness, the greater distance of LMC X-2 relative to similar Galactic sources results in a paucity of photons for high-time-resolution studies.

We have therefore undertaken a program of study of LMC X-2 using RXTE, to search for the orbital period of the system and determine the signature of its fast time variability. We have also obtained simultaneous optical coverage at SAAO with the 1.9m telescope and high-speed CCD photometer, to search for correlated variability between the X-ray and optical regimes; these data will be presented in a later publication (McGowan, Charles, & Smale 1999).

## 2. Observations

We observed LMC X-2 with RXTE (Bradt, Rothschild, & Swank, 1993) between 1997 December 2 18:52 UT – December 7 1:40 UT, for an on-source total good time of 100 ksec. This time was divided into five separate observations, in an observing strategy designed to achieve the maximum amount of simultaneity with the optical coverage mentioned above. The X-ray data we present here were obtained using the PCA instrument with the Standard 2 and Good Xenon configurations, with time resolutions of 16 sec and  $< 1\mu\text{sec}$  respectively. The PCA consists of five Xe proportional counter units (PCUs), with a combined effective area of about  $6500\text{ cm}^2$  (Jahoda et al 1996). All 5 PCUs were on throughout the observations, apart from a 6000-sec interval at the beginning of the third observation during which PCU 4 was turned off. In our light curves we have included the data from this short interval normalized to 5 PCUs.

We performed our data extraction using the RXTE standard data analysis software, FTOOLS 4.2. Background subtraction of the PCA data was performed utilizing the “skyvle/skyactiv” models generated by the RXTE PCA team. The quality of the background subtraction was checked in two ways: (i) by comparing the source and background spectra and light curves at high energies (50–100 keV) where LMC X-2 itself no longer contributes detectable events; and (ii) by using the same models to background-subtract the data obtained during slews to and from the source. We conclude that our background subtractions in the 2–20 keV energy range are accurate to a fraction of a count per second.

We examined the rapid aperiodic variability in LMC X-2 using the high time resolution PCA data obtained in the Good Xenon mode. Discrete power spectral density distributions (PSDs) were calculated by dividing the data into segments of uniform length, performing fast Fourier transforms of each, and averaging the results. The PSDs were normalized such that their integral gives the squared RMS fractional variability (Miyamoto et al 1991; van der Klis 1989). We subtracted the Poisson noise level from the power spectra, taking into account the modifications expected from PCA detector deadtime. As described by Zhang et al (1995, 1996) this deadtime comes in two parts: the  $t_d=10\mu\text{s}$  contribution from the events within in the time series themselves, and a  $\tau=170\mu\text{s}$  contribution from energetic cosmic ray events (very

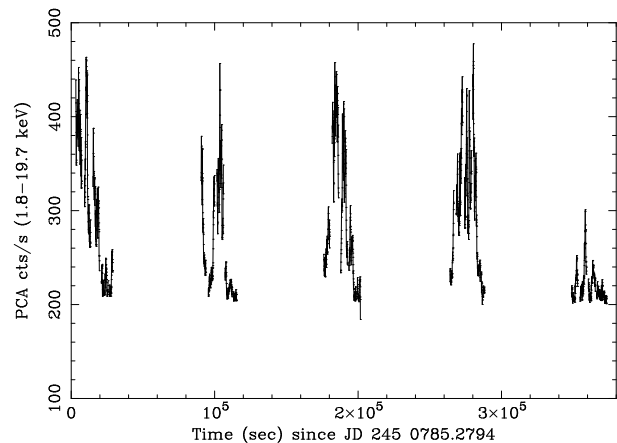


Fig. 1.— Background-subtracted X-ray light curve of LMC X-2, 1997 December 2–7, extracted using an energy range 1.8–19.7 keV and a time resolution of 64 sec.

large events, or VLE) (see also Morgan, Remillard, & Greiner 1997).

Data were also obtained with the HEXTE phoswich detectors, which are sensitive over the energy range 15–250 keV (Rothschild et al. 1998). The source was detected with a background-subtracted count rate of  $0.75\text{ count s}^{-1}$ . However, because of the cut-off spectral shape of LMC X-2, these counts were limited to energies  $< 25\text{ keV}$ , and the HEXTE data did not in this case provide any information additional to that gained using the PCA.

## 3. Results

### 3.1. The light curve and HID/CD

We show the overall 1.8–19.7 keV X-ray light curve in Fig. 1. Pronounced variability is apparent, with some evidence for a modulation on an  $\sim 8\text{ hr}$  timescale in the first four observations, and a suggestion of a similar but much lower-amplitude modulation in the fifth. Using a discrete Fourier transform technique optimized for unevenly-sampled time series (Scargle 1989), we found that the strongest peaks in the power spectrum appear at  $P=29446\pm 147\text{s}$  and the one-day aliases of  $P$  (Fig. 2). No other significant periodicities were detected. The strength and significance of this primary peak is corroborated with a standard period-folding code utilizing the L-statistic (Davies 1990),

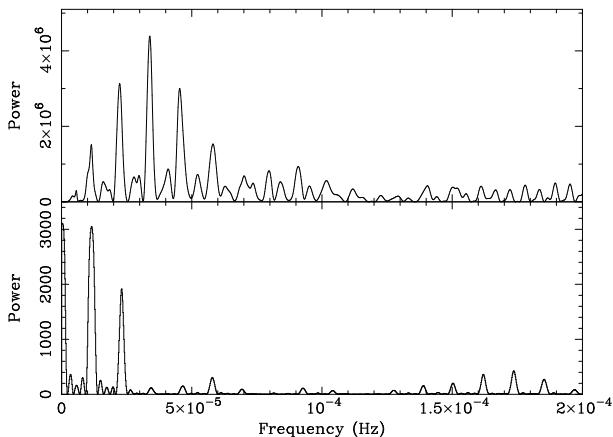


Fig. 2.— The upper panel shows the Fourier power spectrum of the background-subtracted X-ray light curve. The most significant peak corresponds to a period of  $29446 \pm 147$ s; the peaks on either side are the one- and two-day aliases of this fundamental period. The window function, in the lower panel, shows peaks at frequencies corresponding to periods of 1 days and 0.5 days. Fitting sine waves to the raw data, we refine the period determination to  $P=29377 \pm 40$ s  $=8.160 \pm 0.011$  hrs (see text).

with a false alarm probability of less than 0.01%. Aware of the pitfalls of detecting orbital periods in datatrains with individual lengths (in this case averaging 20000s) similar to the period of interest, we have scrutinized the window function of the observations (e.g. van der Klis 1989); from our Fig. 2 we see that the only principal peaks in the window function correspond to the one-day and half-day artefacts from the data sampling. In addition, we have created and analyzed a series of 1000 randomized datasets with the same temporal spacing. None of the randomized datasets showed significant Fourier power or L-statistic peaks in the range of candidate periods of interest ( $\sim$ hrs).

We fine-tuned our measurement of the periodicity in the X-ray data by fitting sine waves to the background-subtracted light curve in Fig. 1, and determining the error on the fitted parameters, producing a final period determination of  $P=29377 \pm 40$ s  $=8.160 \pm 0.011$  hrs. This is startlingly close to the candidate orbital period suggested by Callanan et al. (1990) of  $8.160 \pm 0.024$  hrs, based on optical photom-

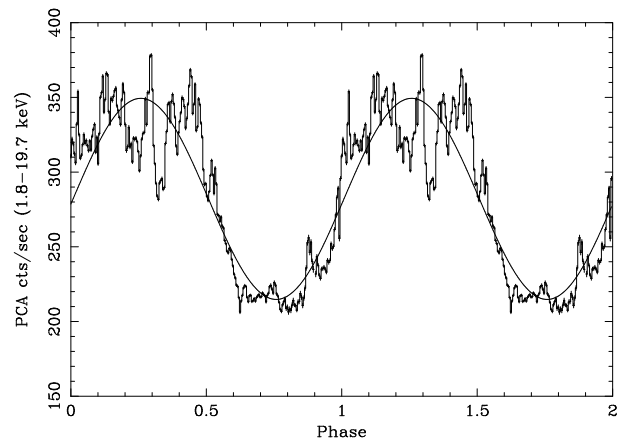


Fig. 3.— The X-ray light curve folded on the candidate orbital period of 29377 sec, with the best-fitting sine wave superimposed over the data. The fifth data segment was excluded before folding. Two cycles are repeated for clarity.

etry. While the close agreement of our analysis with a ten-year-old optical result suggests that the 8.16-hr periodicity is a stable and fundamental cycle of the system, we clearly cannot rule out the possibility of a sequence of flares intrinsic to the source with a fortuitous spacing.

The X-ray lightcurve (excluding the fifth observation) folded on this period is shown in Fig. 3. The epoch of phase zero (defined for the purposes of this paper as the ascending node of the sine wave) is JD 245 0785.279  $\pm$  0.003. The modulation semi-amplitude is 24% over the entire 1.8–19.7 keV range used, increasing linearly with energy from 14% in the 1.8–4.0 keV range to 40% at 8.7–19.7 keV. The modulation during the fifth observation is greatly reduced but still significant, at  $3.8 \pm 0.1\%$  over the 1.8–19.7 keV band. Considerable short-timescale ( $\sim$ minutes) variability is observed in addition to the  $\sim$ 8 hr modulation. Visual inspection of the folded light curve (and detailed study of the individual light curves) indicates that the source shows greater intrinsic X-ray variability at phases  $\phi=0.0-0.5$  than it does at later phases. To quantify this impression, we subtracted the much longer-timescale 8.16-hr modulation from the data and subjected the resulting light curve to a simple statistical analysis: the weighted variance of the folded data is  $\sigma^2=961.9$  between  $\phi=0.0-0.5$ , as

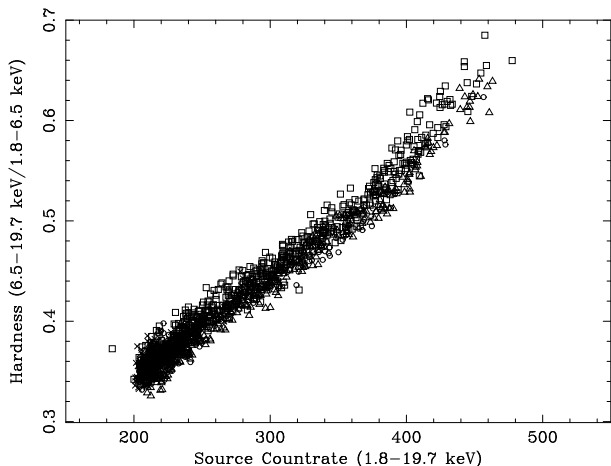


Fig. 4a.— The hardness/intensity diagram for the observation. Data points from the five observing segments are marked using triangles, circles, squares, crosses, and filled squares respectively. Each point represents 64s of data.

compared with  $\sigma^2=129.4$  between  $\phi=0.5$ –1.0.

In Fig. 4 we present the hardness-intensity diagram (HID) and color-color diagram (CD) for the whole observation. The correlation between hardness and intensity is very tight throughout the observations. The CD shows a single straight, cohesive track with a slight hook at the bottom left corner, perhaps indicating a vertex with another branch. For the first four observations the individual hardness-intensity and color-color diagrams are indistinguishable in extent, scatter, and slope; for the fifth observation, the data points cluster in the lower portions of the respective diagrams.

### 3.2. Fast timing characteristics

The overall PSD of the source from 0.01–100 Hz can be well represented using a single power law representing very low frequency ( $\lesssim 1$  Hz) noise (VLFN), with shape  $P \propto \nu^{-\gamma}$ , plus a higher-frequency noise component which we modeled using (i) a cut-off power law, representing standard high frequency ( $\gtrsim 10$  Hz) noise (HFN), or (ii) a Lorentzian, representing peaked HFN. First we examined the mean power spectrum of all the observations, and then investigated it as a function of position in the HID. Fits were performed in several energy ranges: 2–6 keV, 6–20 keV, 20–100

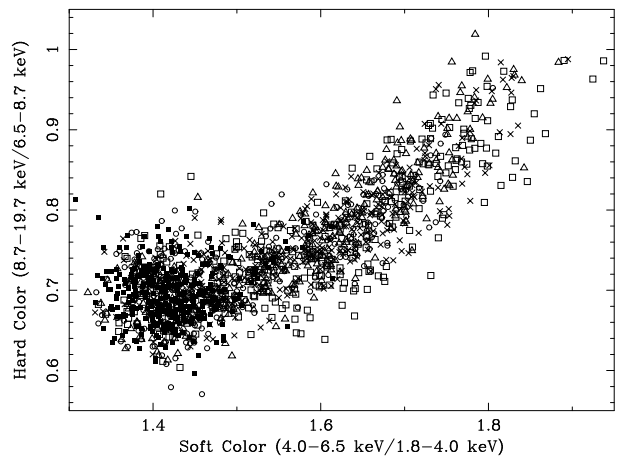


Fig. 4b.— The color-color diagram for the observation. Data points follow the same convention as in Fig. 4a.

keV, and 2–10 keV. The rms values are measured between 0.01–1 Hz for the VLFN and 0.01–100 Hz for HFN, and errors are  $\Delta\chi^2=1.0$ .

In the 2–6 keV power spectrum the VLFN component dominates between 0.01–1 Hz, with best fitting parameters of  $\gamma=1.50\pm 0.07$ ,  $\text{rms}=4.5\pm 0.3\%$ . The best-fitting HFN power law has an index of  $\gamma_H=0.09^{+0.26}_{-0.18}$ ,  $\text{rms}=4.1\pm 0.4\%$ . (The cut-off frequency is found to be beyond the data range.) Adding this second power law improves the quality of the fit from  $\chi^2/dof=105/61$  (VLFN only) to  $\chi^2/dof=81/59$  (VLFN+HFN). In the Lorentzian representation, the center of the peaked noise was found to be  $\nu_H=40\pm 8$  Hz, with  $\text{FWHM}=62^{+43}_{-21}$  Hz,  $\text{rms}=5.1\pm 0.9\%$ ,  $\chi^2/dof=75/58$ . We show a power spectrum and best VLFN+HFN model fit in Fig. 5.

At higher energies, VLFN continues to dominate. In the 6–20 keV spectrum we find  $\gamma=1.56\pm 0.11$ ,  $\text{rms}=4.8\pm 0.3\%$ ,  $\chi^2/dof=89/61$ , with upper limits of  $\text{rms}<1.5\%$  for simple power-law HFN with  $\gamma_H$  fixed at 0.0, and  $\text{rms}<1.4\%$  for peaked HFN with  $\nu_H=40$  Hz,  $\text{FWHM}=60$  Hz. VLFN in the 20–100 keV range is only slightly weaker, with  $\gamma=1.3\pm 0.2$ ,  $\text{rms}=3.9\pm 0.3\%$ ,  $\chi^2/dof=77/61$ , with upper limits of  $\text{rms}<6.0\%$  on HFN.

We detect no quasi-periodic oscillations, and for typical  $Z$ -source NB QPO, with centroid frequency  $\sim 5$  Hz and  $\text{FWHM}$  2–3 Hz, we place a 95% confidence upper limit on the rms of 0.6%. For parameters typi-

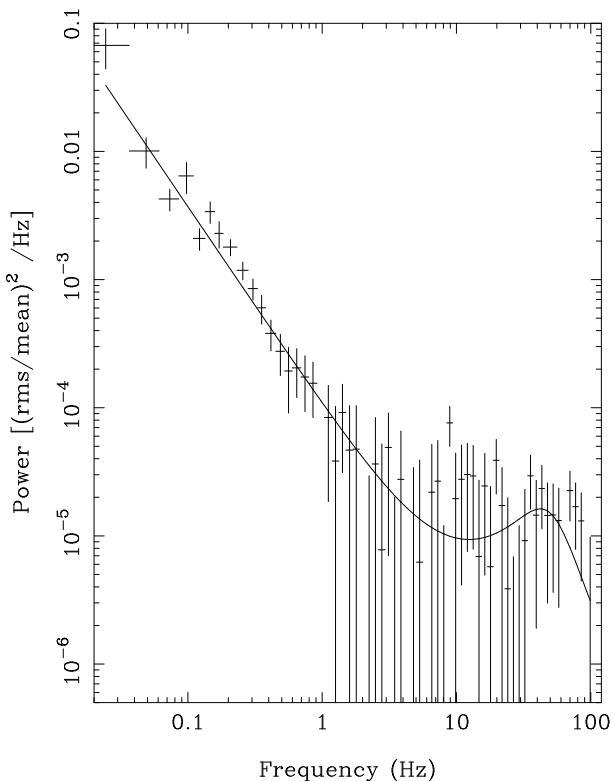


Fig. 5.— The average power spectrum for LMC X-2 in the energy range 2–10 keV. The Poisson level has been subtracted, and the data fitted using a power law plus Lorentzian to characterize the VLFN and HFN components.

cal of *Z*-source FB QPO (centroid frequency ranging from  $\sim 6$  Hz to  $\sim 20$  Hz, with FWHM spanning  $\sim 3$ –20 Hz) or atoll source QPO (frequencies  $\sim 1$ –60 Hz and similar FWHM) we find rms upper limits of  $\sim 1$ –3%.

Power spectra accumulated for each of the first four observations independently show no significant night-to-night change in the strength or slope of the VLFN component, and insufficient statistics to assess variability of the higher-frequency component. We also accumulated power spectra for the 2–10 keV data selected in several broad color-intensity bands along the branch to search for behavioral changes. At overall count rates  $< 250$  c/s we measure  $\gamma = 1.37 \pm 0.16$ , rms =  $3.2 \pm 0.9\%$ , increasing to  $\gamma = 1.63 \pm 0.15$ , rms =  $5.6 \pm 1.5\%$  at intermediate count rates, and  $\gamma = 1.49 \pm 0.10$ , rms =  $3.4 \pm 0.9\%$  at count rates  $> 400$  c/s.

### 3.3. Spectral fitting

The X-ray spectra from LMC X-2 provide a means of parameterizing the variations around the candidate binary cycle. We have examined the summed 2–15 keV spectrum from the whole observation, and also the results of dividing the data into ten spectral bins by phase. The summed spectrum can be well fit using a power law plus high energy cutoff model, with photon index  $\alpha = 0.37 \pm 0.04$  and cutoff energy  $kT = 2.81 \pm 0.04$  keV. In this model, the derived hydrogen column density  $N_H$  is indistinguishable from zero, with an upper limit of  $10^{21}$  cm $^{-2}$ . With 1% systematics added to represent the current uncertainties in the response matrix generation, the goodness of fit is  $\chi^2/dof = 36.8/29$ . The summed data can also be fit using a Comptonized Sunyaev & Titarchuk model with  $N_H = 1.48 \pm 0.32 \times 10^{21}$  cm $^{-2}$ , electron temperature  $kT = 2.00 \pm 0.02$  keV, and scattering depth  $\tau = 14.2 \pm 0.4$ , with a less satisfactory goodness-of-fit of  $\chi^2/dof = 49.6/29$ . To a certain extent these two models can be considered variations on a theme, as both represent the scattering of cool photons on hot electrons; simple Comptonization has been approximated with a cut off power law  $E^{-\alpha} \exp(-E/kT)$  in fits to LMXBs (e.g. White, Peacock, & Taylor 1985, White et al. 1986), while the Sunyaev & Titarchuk model uses the solution to the Kompaneets equation with assumptions about the photon distribution through the scattering cloud (Sunyaev & Titarchuk 1980).

These two models were then fit to the ten phase-resolved spectra from the source. While the cut-off power law is a better fit to the summed spectrum, this is not necessarily the case for the individually-phased spectra; in fact, the Comptonized Sunyaev & Titarchuk model produced a better fit to the data for five out of the ten cases. (Since the summed spectrum is effectively an average over a series of different spectral states, the best-fitting model for individual spectra may not be the model that best fits the summed spectrum.) The variations of the fit parameters with phase are illustrated in Fig. 6. In the first parameterization – the power law plus high energy cutoff – the power law index shows a clear correlation with phase, with the power law slope being at its steepest at minimum light (as might be expected from the larger modulation amplitude observed at higher energies). In contrast, the value of the cutoff temperature does not vary significantly with phase. In the second parameterization – Comptonized Sunyaev & Titarchuk – the electron temperature is similarly insensitive to

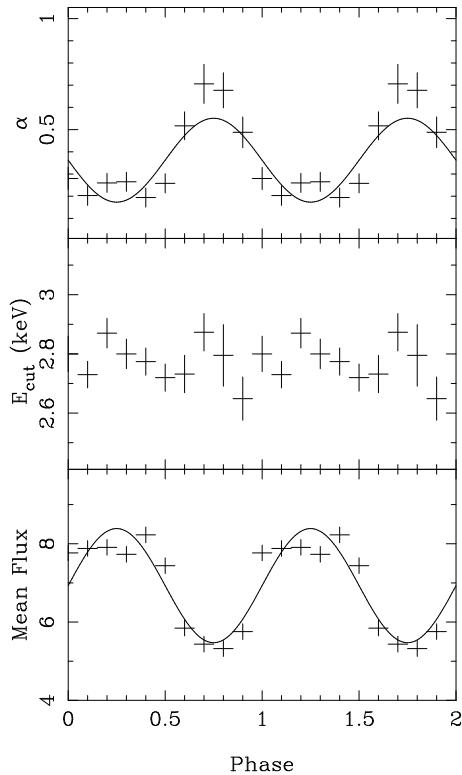


Fig. 6a.— Results of spectral fitting to a series of phase-resolved spectra, showing the variation around the possible binary cycle of the spectral fit parameters for (a) a power law plus high energy cutoff model (b) a Comptonized Sunyaev & Titarchuk model (see text). The mean flux per spectrum is given in units of  $10^{-10}$  erg  $\text{cm}^{-2}$   $\text{s}^{-1}$ . In each case two cycles are shown for clarity.

phase, while the depth to optical scattering  $\tau$  shows a positive correlation. However, since the upscattering is believed to take place in the immediate vicinity of the neutron star, the physical interpretation of such a dependence is not clear.

We have also fit a series of combination models to the data, chief among them a cutoff power law plus blackbody, Bremsstrahlung plus blackbody, a pair of blackbodies, and a disk-blackbody plus blackbody. None of these combinations applied to the spectral data provided an overall goodness-of-fit statistically superior to the single-component Comptonization models, and in most cases the fits themselves were insufficiently stable to determine meaning-

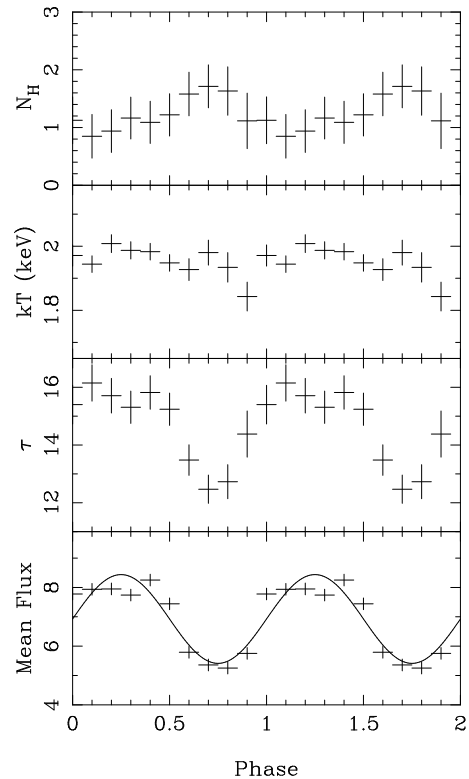


Fig. 6b.— See caption for Fig. 6a.

ful error estimates. Of the combination models, the Bremsstrahlung plus blackbody fit provided the best description of the data (despite being perhaps the least physically realistic, due to the large emitting volumes required), with parameters  $kT_{Brems}=4.5$  keV,  $kT_{BB}=1.5$  keV,  $\chi^2/dof=32/28$ , with the blackbody making up  $\sim 20\%$  of the total flux. However, fitting the phase-selected spectra with this model we found the fit parameters were not independent, in the sense that the Bremsstrahlung temperature, the blackbody temperature, the derived blackbody flux, and the proportion of the total flux made up by the black body all increased with increasing flux in a correlated fashion. This interdependency of unrelated fit parameters is typical when fitting models that are over-defined. We note that Bonnet-Bidaud et al. (1989) had similar difficulties correlating the fit parameters for a Bremsstrahlung plus black body model with the flux level of the source.

At the 50 kpc distance of the LMC, the mean observed flux translates to a source luminosity of



$1.8 \times 10^{38}$  erg s<sup>-1</sup>, in the middle of its known historical luminosity range. For a standard  $1.4M_{\odot}$  neutron star binary with cosmic abundances this is equivalent to the Eddington luminosity.

## 4. Discussion

### 4.1. LMC X-2: $Z$ or atoll?

LMC X-2 has never been explicitly assigned to either the  $Z$  or the atoll class of sources, but our results suggest that it is either a bona fide  $Z$ -source, or an anomalous atoll source with many  $Z$ -source characteristics.

The first consideration is the high luminosity of the source. Atoll sources have absolute luminosities that range from  $0.01$ – $0.1L_{Edd}$  for the X-ray burst sources, up to  $0.1$ – $0.3L_{Edd}$  for the bright GX atoll sources (e.g. GX 9+9, GX 13+1). The known  $Z$ -sources radiate consistently at a large fraction of the Eddington luminosity, and frequently exceed that luminosity for extended intervals. From their modeling of the spectral variability of  $Z$ -sources, Psaltis et al. (1995) find internally self-consistent solutions with accretion rates on the NB of  $0.9$ – $1.0\dot{M}_{Edd}$ , and rates  $> \dot{M}_{Edd}$  on the FB. The luminosity of LMC X-2 exceeds that of the bright atoll sources by a factor of several, historically spanning the range  $\sim 0.4$ – $2.0L_{Edd}$ , with a mean luminosity of  $\sim 1.0L_{Edd}$  at the time of our observations. LMC X-2 also shows intervals of flaring behavior (e.g. Bonnet-Bidaud et al. 1989; this paper), a frequently-observed characteristic of many  $Z$ -sources.

Secondly, the CD and HID of LMC X-2 show many similarities with diagrams generated for confirmed  $Z$ -sources. In particular they strongly resemble those sometimes observed from GX 349+2 in its flaring branch (Hasinger & van der Klis 1989; Kuulkers & van der Klis 1995), with a straight, tightly-correlated HID and an almost equally straight and focussed CD. The concentration and distribution of points in the lower left of the CD and HID in both sources suggest the vertex with an incipient normal branch (seen explicitly in later observations of GX 349+2: Kuulkers & van der Klis 1998; Zhang, Strohmayer, & Swank 1998). By contrast, most atoll sources show pronounced curvature in their banana branch (Schulz et al. 1989, Hasinger & van der Klis 1989, Prins & van der Klis 1997, among others) and a more diffuse distribution of data points (see e.g. the atoll plots constructed using RXTE PCA data from 4U1735-444, Wijnands et al. 1998; 4U1608-52; Méndez et al.

1999). Among the atoll-sources only the bright galactic center sources GX 9+9 and GX 13+1 show a CD and HID comparable to that of LMC X-2 (Hasinger & van der Klis 1989; Homan et al. 1998), and neither source does this consistently (see e.g. Schulz et al. 1989).

$Z$  and atoll sources are classified using a combination of CD/HID evidence and the results of fast timing analysis. The power spectra of both source classes contain VLFN, with power law indices generally  $\gamma=1.2$ – $1.4$  for atoll sources and  $\gamma > 1.5$  for  $Z$ -sources in the flaring branch (e.g. Hasinger & van der Klis 1989; Kuulkers 1995; Prins & van der Klis 1997), although there are occasional exceptions (e.g. KS1731-260,  $\gamma=1.5$ , Wijnands & van der Klis 1997). The measured values for LMC X-2 of  $\gamma=1.5$ – $1.7$  fall within the range observed for  $Z$ -sources. More compelling than the absolute value of the power law index is the overall fast behavior of the source as it travels along its branch. In the atoll sources the power spectrum is generally dominated by HFN in the lower banana, and by VLFN in the upper banana (e.g. van der Klis 1995; Prins & van der Klis 1997). By contrast, VLFN dominates all along the observed branch of LMC X-2.

Close attention to the phenomenology of the VLFN is generally not a high priority in studies of  $Z$ -sources, but we note that for Cyg X-2 at high overall intensity, the LFN decreases and disappears on the lower NB, while the VLFN remains strong and steep along the FB (Wijnands et al. 1997). Steep power-law VLFN is similarly observed in the low state of Cyg X-2 (Kuulkers, Wijnands, & van der Klis 1999). The VLFN in Sco X-1 increases in strength as the source travels from the NB/FB vertex to the end of the FB from rms=2% to 6%, with an almost-constant power-law index of  $\gamma_{Sco}=1.72 \pm 0.01$ , while the HFN peaks at rms=3.0% and then fades into undetectability (Hertz et al. 1992). Along the FB, Cir X-1 is similarly dominated by VLFN (Shirey et al. 1998, 1999). In both  $Z$  and atoll sources there are indications that the power law steepens as the source moves upward and rightward in the CD (along the flaring branch, or from lower to upper banana), a trend also (partially) observed in LMC X-2. Where observed, the HFN in  $Z$ -sources typically has  $\gamma \sim 0$  and a cut-off frequency approaching 100 Hz, consistent with the HFN observed in LMC X-2. If LMC X-2 is a  $Z$ -source we might expect the presence of NBO/FBO; none were found, although our upper limits are consistent with the de-

tection levels for such QPO in other  $Z$ -sources.

#### 4.2. The orbital periodicity

We have detected an apparent strong 8.16-hr orbital periodicity in the X-ray flux during four observations of LMC X-2, with an average modulation amplitude of 24% across the 1.8-19.7 keV energy band. In the fifth observation, this amplitude has dropped to 4% over the same energy band. This variability in the modulation depth, coupled with the intrinsic variability of the source, may explain why the periodicity is not evident in the public archival data from the all-sky monitor instruments on RXTE, Vela 5-B, and Ariel V. The pointed observations of LMC X-2 from previous X-ray missions stored in the HEASARC online archive are too short to allow a search for a  $\sim$ 8-hr periodicity; the longest observation, performed using EXOSAT on 1985 December 10, lasts 18 hrs and shows 20% variability, but no clear orbital modulation. The majority of LMXBs have orbital periods of 2–10 hrs. If the 8-hr period were confirmed as orbital, LMC X-2 would fall towards the upper end of this distribution, implying a dwarf companion of  $\sim 1M_{\odot}$  perhaps beginning to evolve off the main sequence, with mass transfer starting to be driven by evolution of the companion.

While the coincidence of the close agreement between the photometric and X-ray periodicities is impressive, we strongly advise caution. Given the sampling of our data we cannot rule out the possibility of a fortuitous alignment of flare episodes, mimicking a true period determination. We note that such an alignment previously produced an erroneous period determination of 8.71 days in GX 349+2 (Ponman 1982). (The true period of 22.5 hr was identified from optical photometry: Wachter 1997.)

In addition, the physical mechanism that might produce such a large modulation in the orbital light curve is by no means clear. At X-ray and optical energies, the shape of the observed light curves in LMXBs, and the existence of an observable modulation, depend strongly upon the inclination  $i$ , and the thickness and geometry of the accretion disk. At high inclinations ( $i > 80^{\circ}$ ) the central source is obscured by the disk edge and the observed X-rays are scattered through an accretion disk corona, producing a light curve with a smooth sinusoidal modulation, interrupted by a partial eclipse of the ADC by the companion (White & Holt 1982, Mason & Córdova 1982). At inclinations ( $75^{\circ} < i < 80^{\circ}$ ) the central source is

often directly visible, and the  $L_x/L_{opt}$  ratio thus significantly enhanced. Sharp regular eclipses by the companion are observed, along with deep irregularly-shaped dips caused by the occultation of the central source by azimuthal structure on the accretion disk associated with the impact point of the accretion stream on the disk edge (e.g. X0748–676; Parmar et al. 1986). At  $70^{\circ} < i < 75^{\circ}$ , X-ray dips are observed but no eclipses, and optical light curves become roughly sinusoidal, with minima occurring 0.2 in phase after the dips (e.g. X1254–690; Courvoisier et al. 1986, Motch et al. 1987). At inclinations lower than  $70^{\circ}$  we cease to see eclipses or dips, and the optical light curves are generally sinusoidal (e.g. X1735–444, X1636–536, Corbet et al. 1986, Smale & Mukai 1988) with the exception of those sources in which ellipsoidal variations are observed from giant companions.

The large-amplitude, quasi-sinusoidal X-ray modulation observed from LMC X-2 does not fit neatly into this picture. The deeper parts of the folded light curve are not associated with a dramatic increase in the  $N_H$ , as is generally the case for a source in which the azimuthal structure plays a major role in defining the modulation, and the amplitude of the modulation itself is clearly not stable, indicating a volatile origin. Neither sharp nor partial eclipses are observed, thereby limiting the source inclination to  $< 75^{\circ}$ . If real, this would suggest that either the periodicity originates in: (a) some modulation of the mass accretion rate itself (noting that the variations in mass accretion are also responsible for the variations of the source along the branches of the CD/HID), or (b) modulation of the flux by the azimuthal disk structure according to the accepted model for dipping sources, requiring that the source inclination falls in the narrow  $70 < i < 75^{\circ}$  band. We note that the intrinsic X-ray luminosity of LMC X-2 is an order of magnitude greater than the luminosities of the Galactic dipping sources, leaving us with no precedent for such a system, and that no good physical model exists for the height and distribution of the obscuring material at the disk's edge even for the lower-luminosity dipping sources.

In previous work, evidence has been presented in favor of a 12.5-day periodicity, based on optical photometry of LMC X-2 (Crampton et al. 1990). Radial velocity measurements are inconclusive, and this longer period is not seen in the RXTE ASM light curve. In LMXBs with known periods in excess of a

few days such as 4U0921–630 (8.99 days, and Cygnus X–2 (9.84 days) the evolved giant companions can be independently detected from the late-type absorption spectrum underlying the strong emission-line spectrum from the accretion disk (Cowley, Crampton, & Hutchings 1982; Cowley, Crampton, & Hutchings 1979), whereas spectroscopic studies of LMC X–2 have as yet provided no evidence for spectral features from the secondary star (Crampton et al. 1990, Bonnet-Bidaud et al. 1989) even in the near-infrared, where we might expect to see Ca II absorption at  $\lambda 8500\text{\AA}$  (Cowley et al. 1991). However, we cannot at this time discount the possibility of a 12.5-day modulation in the system, as superorbital periodicities have been detected in several LMXBs (e.g. 175 days in 4U1820–303, 199 days in 4U1916–053, see Smale & Lochner 1992, and references therein; 78 days in Cyg X–2, Wijnands, Kuulkers, & Smale 1996) perhaps due to precession of a tilted accretion disk. A program of long-term optical photometry of LMC X–2 is currently under way to resolve this question (Wachter, Greene, & Smale 1999).

An empirical relation exists between the absolute visual magnitude  $M_V$  of a LMXB, its mean X-ray luminosity as a function of  $L_{Edd}$ , and its orbital period (van Paradijs & McClintock 1994). (Such a relationship is expected from a simple model where the bulk of the optical emission comes from – and scales with the size of – a standard accretion disk.) Given a  $V$ -magnitude of 18.5 for LMC X–2 and a reddening of  $E_{B-V}=0.1$  (which agrees well with the  $N_H$  expected from interstellar absorption in the direction of the LMC; Bonnet-Bidaud et al. 1989), the derived absolute magnitude of  $-0.3$  leads to an expected orbital period of  $\sim 17_{-8}^{+10}$  hrs. If our detected 8-hr periodicity does not stand the test of time, future (X-ray or optical) search strategies should still be focused on the 8–30 hr domain.

## 5. Conclusion

From this first study of the fast timing and CD/HID properties of LMC X–2 we have accumulated evidence that suggests it might be a  $Z$ -source. Considerations of the sustained near-Eddington and super-Eddington luminosity, the shape and other characteristics of the color-color diagram, and the fast time variability over the 0.01–100 Hz range all seem to support the hypothesis. If true, we might expect to observe different branches of the  $Z$  in future observations of the source,

perhaps while in intensity states differing from those observed here.

$Z$ -sources may fall into two classes, based on their inclination (e.g. Kuulkers & van der Klis 1995). Sco X–1, GX 349+2, and GX 17+2 show stable  $Z$ s in their CDs and increase in brightness along the FB, and may be observed at low inclination. By contrast, Cyg X–2, GX 340+0, and GX 5–1 all show pronounced secular variations in the positions of their  $Z$ s in the CD, and their brightnesses show decreases or only slight increases along the FB (where observed); these sources are believed to be observed at high inclination. If a  $Z$ -source, LMC X–2 would probably join the first class based on its FB behavior, adding even further to the difficulty of creating a sustained high-amplitude orbital modulation in its X-ray light curve.

This research has made use of data obtained through the High Energy Astrophysics Science Archive Research Center Online Service, provided by the NASA Goddard Space Flight Center. We acknowledge helpful conversations with Rudy Wijnands, Stefanie Wachter, Phil Charles, & Katie McGowan.

## REFERENCES

- Bonnet-Bidaud, J. M., Motch, C., Beuermann, K., Pakull, M., Parmar, A. N., & van der Klis, M., 1989, *A&A*, 213, 97
- Bradt, H. V., Rothschild, R. E., & Swank, J. H., 1993, *A&AS*, 97, 355
- Callanan, P. J., Charles, P. A., van Paradijs, J., van der Klis, M., Pedersen, H., & Harlaftis, E. T., 1990, *A&A*, 240, 348
- Corbet, R. H. D., Thorstensen, J. R., Charles, P. A., Menzies, J. W., Naylor, T., & Smale, A. P., 1986, *MNRAS*, 222, 15P
- Courvoisier, T. J.-L., Parmar, A. N., Peacock, A., & Pakull, M., 1986, *ApJ*, 309, 265
- Cowley, A. P., Crampton, D., & Hutchings, J. B., 1979, *ApJ*, 231, 539
- Cowley, A. P., Crampton, D., & Hutchings, J. B., 1982, *ApJ*, 256, 605
- Cowley, A. P., Schmidtke, P. C., Crampton, D., Hutchings, J.B., & Bolte, M., 1991, *ApJ*, 373, 228
- Crampton, D., Cowley, A. P., Hutchings, J. B., Schmidtke, P. C., & Thompson, I. B., 1990, *ApJ*, 355, 496

- Davies, S. R., 1990, MNRAS, 244, 93
- Griffiths, R. E. & Seward, F. D., 1977, MNRAS, 180, 75P
- Hasinger, G., & van der Klis, M., 1989, A&A, 225, 79
- Hertz, P., Vaughan, B., Wood, K. S., Norris, J. P., Mitsuda, K., Michelson, P. F., & Dotani, T., 1992, ApJ, 396, 201
- Homan, J., van der Klis, M., Wijnands, R., Vaughan, B., & Kuulkers, E., 1998, ApJ, 499, L41
- Jahoda, K., Swank, J. H., Giles, A. B., Stark, M. J., Strohmayer, T., Zhang, W., & Morgan, E. H., 1996, in EUV, X-ray and Gamma-Ray Instrumentation for Astronomy VII, ed O. H. Siegmund (Bellingham, WA: SPIE), 59
- Johnston, M. D., Bradt, H. V., & Doxsey, R. E., 1979, ApJ, 233, 514
- Jonker, P. G., van der Klis, M., & Wijnands, R., 1999, ApJ, 511, L41
- Kuulkers, E., 1995, PhD thesis, University of Amsterdam
- Kuulkers, E., & van der Klis, M., 1995, Ann.New York.Ac.Sci, 759, 344
- Kuulkers, E., & van der Klis, M., 1998, A&A 332, 845
- Kuulkers, E., Wijnands, R., & van der Klis M., 1999, MNRAS, in press: astro-ph/9904352
- Long, K. S., Helfand, D. J., & Grabelsky, D. A., 1981, ApJ, 248, 925
- Mason, K. O., & Córdova, F. A., 1982, ApJ, 262, 253
- McGowan, K., Charles, P. A., & Smale, A. P., 1999, in preparation
- Méndez, M., van der Klis, M., Ford, E. C., Wijnands, R., van Paradijs, J., 1999, ApJ, 511, L49
- Miyamoto, S., Kimura, K., Kitamoto, S., Dotani, T., & Ebisawa, K., 1991, ApJ, 383, 784
- Morgan, E. H., Remillard, R. A., & Greiner, J., 1997, ApJ, 482, 993
- Motch, C., Pedersen, H., Courvoisier, T. J.-L., Beuerman, K., & Pakull, M. W., 1987, ApJ, 313, 792
- Parmar, A. N., White, N. E., Giommi, P., & Gottwald, M., 1986, ApJ, 308, 199
- Ponman, T., 1982, MNRAS, 200, 351P
- Prins, S., & van der Klis, M., 1997, A&A, 319, 498
- Psaltis, D., Lamb, F. K., & Miller, G. S., 1995, ApJ, 454, L137
- Rothschild, R. E., Blanco, P. R., Gruber, D. E., Heindl, W. A., MacDonald, D. R., Marsden, D. C., Pelling, M. R., & Wayne, L. R., 1998, ApJ, 496, 538
- Scargle, J. D., 1989, ApJ, 343, 874
- Schulz, N. S., Hasinger, G., & Truemper, J., 1989, A&A, 225, 48
- Shirey, R. E., Bradt, H. V., & Levine, A. M., 1999, ApJ in press (astro-ph/9901003)
- Shirey, R. E., Bradt, H. V., Levine, A. M., & Morgan, E. H., 1998, ApJ, 506, 374
- Smale, A. P., & Lochner, J. C., 1992, ApJ, 395, 582
- Smale, A. P., & Mukai, K., 1988, MNRAS, 231, 663
- Sunyaev, R. A., & Titarchuk, L. G., 1980, A&A, 86, 121
- van der Klis, M., 1989, in Timing Neutron Stars, H. Ogelman & E. P. J. van den Heuvel (eds), Cambridge University Press, p. 252
- van der Klis, M. 1995, in X-ray Binaries, W. H. G. Lewin, J. van Paradijs, & E. P. J. van den Heuvel (eds.), Cambridge University Press, 252
- van der Klis, M. 1998, in The Many Faces of Neutron Stars, R. Buccheri, J. van Paradijs, & M. A. Alpar (eds), Kluwer, Dordrecht, NATO ASI Series C, 515, 337
- van Paradijs, J., 1995, in X-ray Binaries, W. H. G. Lewin, J. van Paradijs, & E. P. J. van den Heuvel (eds.), Cambridge University Press, 536
- van Paradijs, J., & McClintock, J. E., 1994, A&A, 290, 133
- Wachter, S., 1997, ApJ, 490, 401
- Wachter, S., Greene, J., & Smale, A. P., in preparation
- White, N. E., & Holt, S. S., 1982, ApJ, 257, 318
- White, N. E., Peacock, A., Hasinger, G., Mason, K. O., Manzo, G., Taylor, B. G., & Branduardi-Raymont, G., 1986, MNRAS, 218, 129
- White, N. E., Peacock, A., & Taylor, B. G., 1985, ApJ, 296, 475
- Wijnands, R. A. D., Kuulkers, E., & Smale, A. P., 1996, ApJ, 473, L45
- Wijnands, R. A. D., & van der Klis, M., 1997, ApJ, 482, L65

- Wijnands, R. A. D., & van der Klis, M., 1999, ApJ, 514, 939
- Wijnands, R. A. D., van der Klis, M., Kuulkers, E., Asai, K., & Hasinger, G., 1997, A&A, 323, 399
- Wijnands, R. A. D., van der Klis, M., Méndez, M., van Paradijs, J., Lewin, W. H. G., Lamb, F. K., Vaughan, B., & Kuulkers, E., 1998, ApJ, 495, L39
- Wijnands, R. van der Klis, M., & Rijkhorst, E.-J., 1999, ApJ, in press (astro-ph/9812244)
- Zhang, W., Jahoda, K., Swank, J. H., Morgan, E. H., & Giles, A. B., 1995, ApJ, 449, 930
- Zhang, W., Morgan, E. H., Jahoda, K., Swank, J. H., Strohmayer, T. E., Jernigan, G., & Klein, R. I., 1996, ApJ, 469, L29
- Zhang, W., Strohmayer, T. E., & Swank, J. H., 1998, ApJ, 500, L167